Supplementary Information

Dimensional crossover of correlated anion disorder in oxynitride perovskites

Hannah Johnston, Ashley P. Black, Paula Kayser Gonzalez, Judith Oró-Solé, David A. Keen, Amparo Fuertes, and J. Paul Attfield

Table S1 Chemical analysis of nitrogen contents for $Ba_{1-x}Sr_xTaO_2N$ samples.

x	N content
0.0	0.97
0.2	0.95
0.4	0.96
0.6	0.97
0.8	0.99
1.0	0.98

Table S2 Refined neutron atomic parameters for cubic $Pm\bar{3}m$ (x = 0 - 0.2) and tetragonal $P4/mmm$ (x = 0.4 - 1) refinement models of $Ba_{1-x}Sr_xTaO_2N$ solid solutions at 300 K. Isotropic thermal parameter Uiso values have $Å^2$ units. Occupancies >100% are shown for x = 0.8 and 1.0 refinements to demonstrate the precision and accuracy of the refinements.

$BaTaO_2N$ $Pm\bar{3}m$ refinement

	x	y	z	Uiso	Occ
Ba	0.5	0.5	0.5	0.3(1)	1
Ta	0	0	0	0.4(1)	1
O	0	0	0.5	0.6(1)	0.667
N	0	0	0.5	0.6(1)	0.333

$Ba_{0.8}Sr_{0.2}TaO_2N$ $Pm\bar{3}m$ refinement

	x	y	z	Uiso	Occ
Ba	0.5	0.5	0.5	0.5(1)	0.8
Sr	0.5	0.5	0.5	0.5(1)	0.2
Ta	0	0	0	0.9(1)	1
O	0	0	0.5	0.88(9)	0.667
N	0	0	0.5	0.88(9)	0.333

$Ba_{0.6}Sr_{0.4}TaO_2N$ $P4/mmm$ refinement

	x	y	z	Uiso	Occ
Sr	0.5	0.5	0.5	0.8(1)	0.4
Ba	0.5	0.5	0.5	0.8(1)	0.6
Ta	0	0	0	1.0(1)	1
O	0	0	0.5	1.14(8)	0.93(1)
N	0	0	0.5	1.14(8)	0.01(1)
O	0.5	0	0	1.14(8)	0.54(5)
N	0.5	0	0	1.14(8)	0.46(5)

$Ba_{0.4}Sr_{0.6}TaO_2N$ $P4/mmm$ refinement

	x	y	z	Uiso	Occ
Sr	0.5	0.5	0.5	0.52(5)	0.6
Ba	0.5	0.5	0.5	0.52(5)	0.4
Ta	0	0	0	0.52(5)	1
O	0	0	0.5	0.84(5)	0.99(3)
N	0	0	0.5	0.84(5)	0.03(3)
O	0.5	0	0	0.84(5)	0.52(1)
N	0.5	0	0	0.84(5)	0.48(1)

$Ba_{0.2}Sr_{0.8}TaO_2N$ $P4/mmm$ refinement

	x	y	z	Uiso	Occ
Sr	0.5	0.5	0.5	0.32(6)	0.2
Ba	0.5	0.5	0.5	0.32(6)	0.8
Ta	0	0	0	0.30(7)	1
O	0	0	0.5	0.75(6)	1.04(3)
N	0	0	0.5	0.75(6)	-0.05(3)
O	0.5	0	0	0.75(6)	0.49(2)
N	0.5	0	0	0.75(6)	0.51(2)

$SrTaO_2N$ $P4/mmm$ refinement

	x	y	z	Uiso	Occ
Sr	0.5	0.5	0.5	0.62(5)	1
Ta	0	0	0	0.52(6)	1
O	0	0	0.5	1.40(6)	1.02(3)
N	0	0	0.5	1.40(6)	-0.03(3)
O	0.5	0	0	1.40(6)	0.49(1)
N	0.5	0	0	1.40(6)	0.51(1)

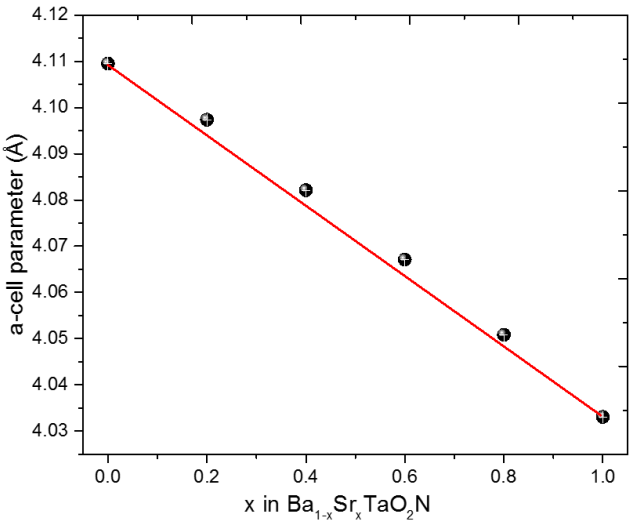

Fig. S1. Plot of cubic or pseudocubic 300 K lattice parameters for $Ba_{1-x}Sr_xTaO_2N$ solid solutions against x.

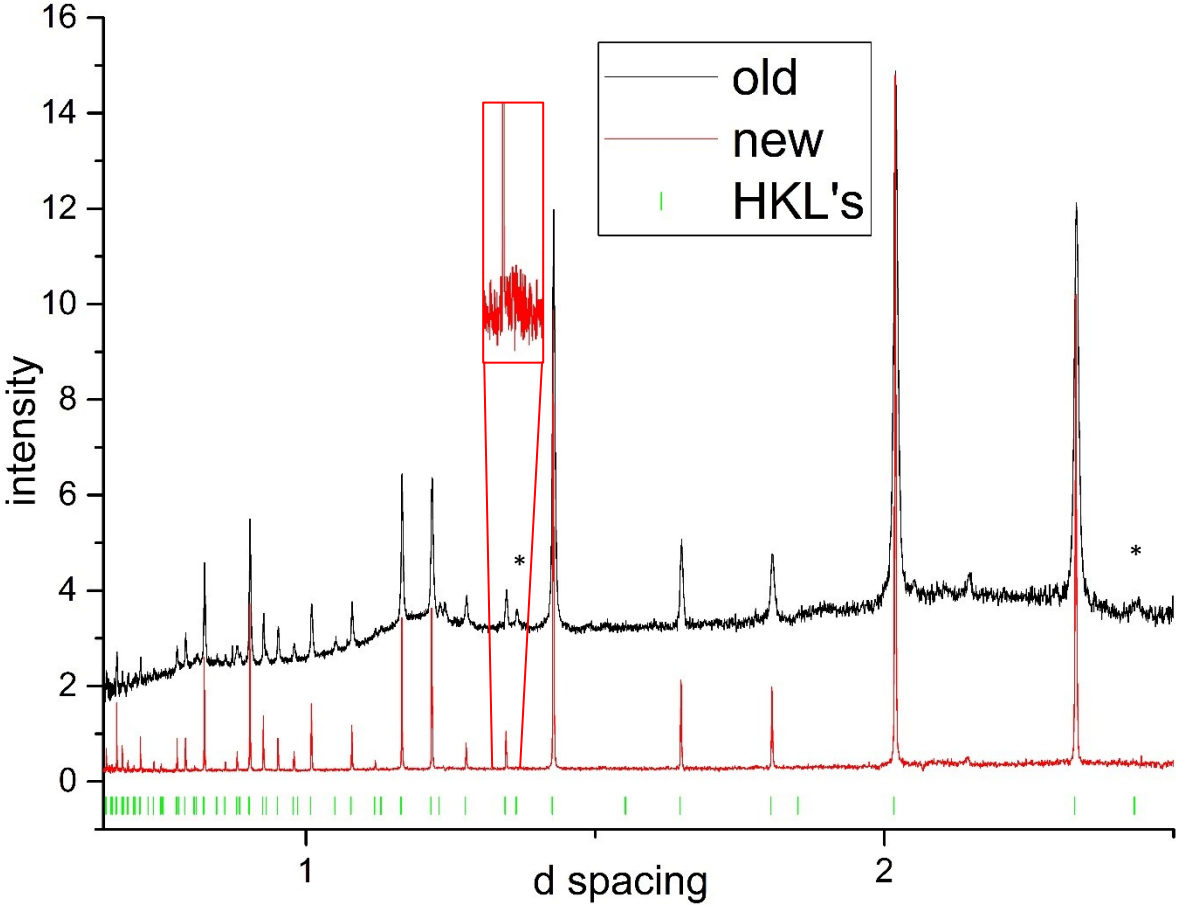

Fig. S2. Comparison of HRPD powder neutron diffraction profiles from the 'new' $SrTaO_2N$ sample used in the present study, and the 'old' sample used in ref. 7. (The 'old' sample was contained in a silica tube giving rise to the observed background scatter.) Peaks at d = 2.45 and 1.36 Å marked * from a rotational *Fmmm* superstructure of octahedral tilts are evident in the old data, but are extensively broadened for the new sample (the broadened 1.36 Å peak is shown in the inset) demonstrating that rotational domains are small. Hence the new data are analysed using a *P4/mmm* model without octahedral rotations, as described in the main text.

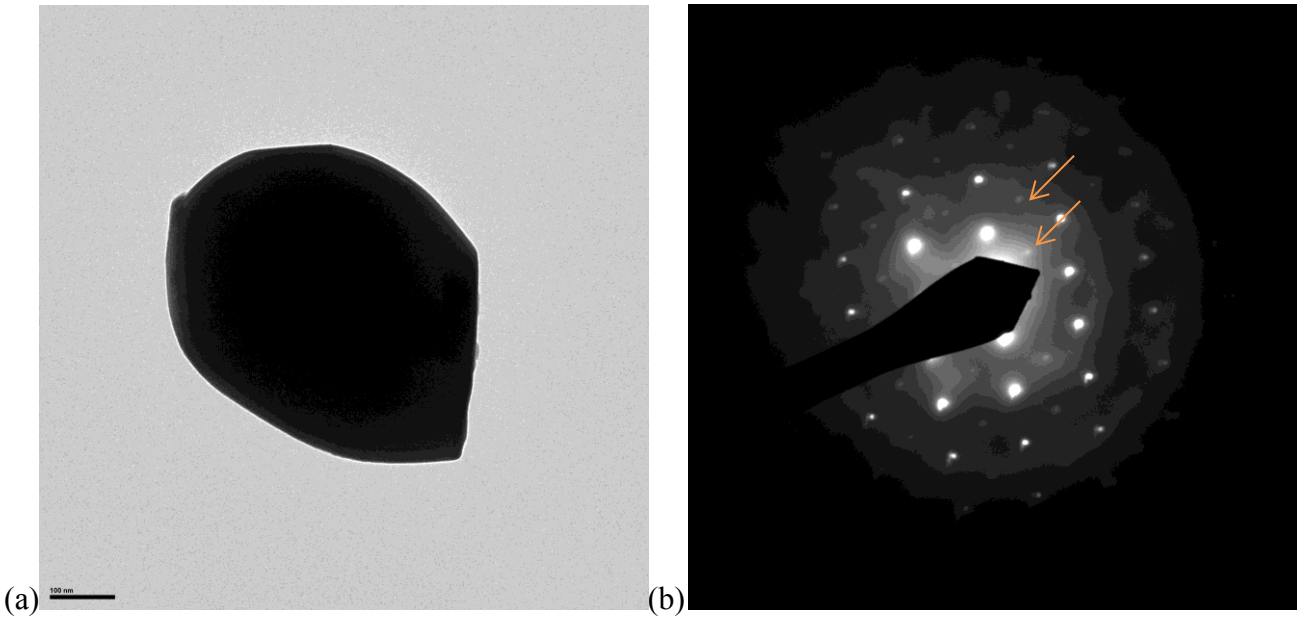

Fig. S3. Electron microscopy results for the $SrTaO_2N$ sample. (a) A typical grain – scale bar is 0.1 μm. (b) Electron diffraction pattern from the grain with weak superstructure peaks characteristic of tilt domains arrowed.

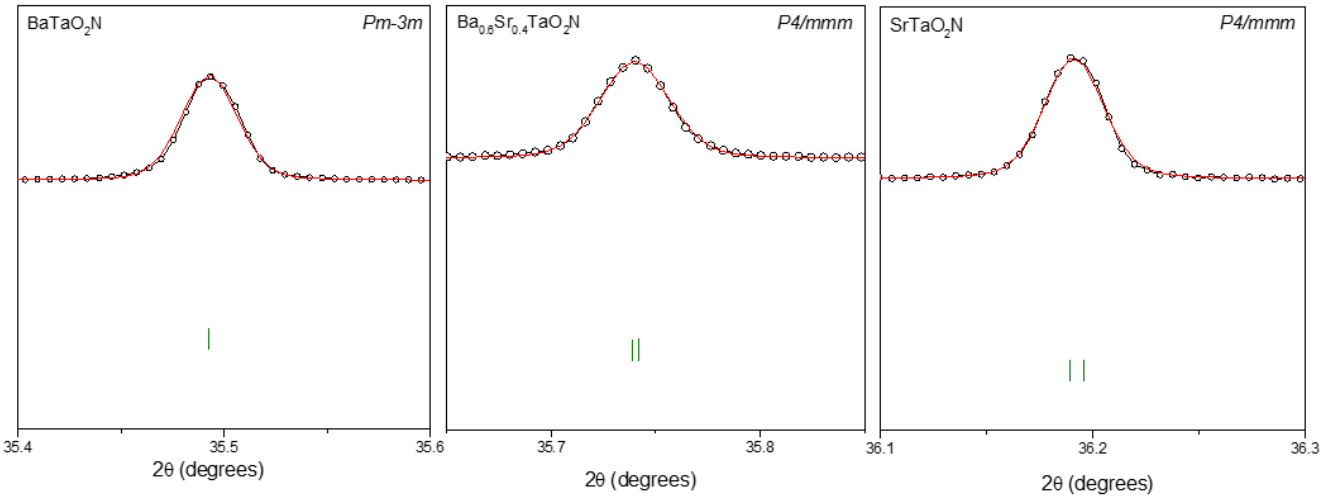

(a) (b) (c)

Fig. S4. Blow-ups of the fitted (400) synchrotron X-ray diffraction peak in the $Ba_{1-x}Sr_xTaO_2N$ series. (a) cubic x = 0 with no microstrain broadening or tetragonal distortion, (b) x = 0.4 showing microstrain broadening due to Ba/Sr mixing and tetragonal distortion, and (c) x = 1 where microstrain broadening is minimal and tetragonal splitting leads to a slight shoulder at the high-2θ side.

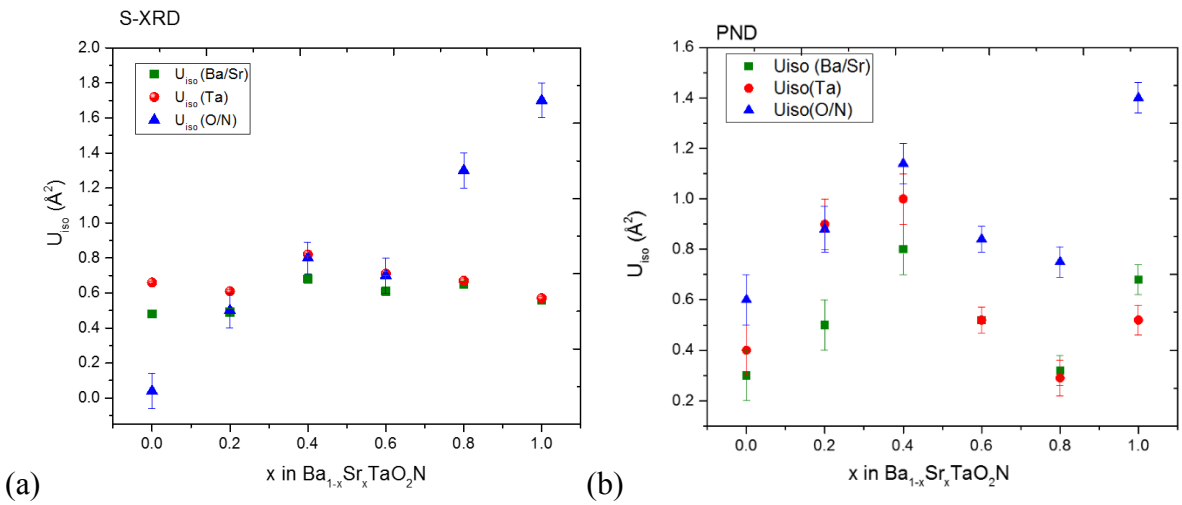

Fig. S5. Plots of refined Uiso's across the $Ba_{1-x}Sr_xTaO_2N$ series from (a) synchrotron and (b) neutron refinements.